

## Time-resolved gamma spectroscopy of single events

Wolszczak, W.; Dorenbos, P.

**DOI**

[10.1016/j.nima.2017.12.080](https://doi.org/10.1016/j.nima.2017.12.080)

**Publication date**

2018

**Document Version**

Accepted author manuscript

**Published in**

Nuclear Instruments and Methods in Physics Research, Section A: Accelerators, Spectrometers, Detectors and Associated Equipment

**Citation (APA)**

Wolszczak, W., & Dorenbos, P. (2018). Time-resolved gamma spectroscopy of single events. *Nuclear Instruments and Methods in Physics Research, Section A: Accelerators, Spectrometers, Detectors and Associated Equipment*, 886, 30-35. <https://doi.org/10.1016/j.nima.2017.12.080>

**Important note**

To cite this publication, please use the final published version (if applicable). Please check the document version above.

**Copyright**

Other than for strictly personal use, it is not permitted to download, forward or distribute the text or part of it, without the consent of the author(s) and/or copyright holder(s), unless the work is under an open content license such as Creative Commons.

**Takedown policy**

Please contact us and provide details if you believe this document breaches copyrights. We will remove access to the work immediately and investigate your claim.

# Time-resolved gamma spectroscopy

W. Wolszczak, P. Dorenbos

*Delft University of Technology, Faculty of Applied Sciences, Department of Radiation  
Science and Technology (FAME-LMR), Mekelweg 15, 2629 JB Delft, Netherlands*

---

## Abstract

In this article we present a method of characterizing scintillating materials by digitization of each individual scintillation pulse followed by digital signal processing. With this technique it is possible to measure the pulse shape and the energy of an absorbed gamma photon on an event-by-event basis. In contrast to other methods, the digital approach provides a shorter measurement time, an active noise suppression, and enables characterization of scintillation pulses simultaneously in two domains: time and energy. We applied this method to study the pulse shape change of a CsI(Tl) scintillator with energy of gamma excitation. We confirmed previously published results and revealed new details of the phenomenon.

*Keywords:* time-resolved gamma spectroscopy, pulse shape analysis, data acquisition, digital signal processing, gamma spectroscopy, CsI(Tl)

---

## 1. Introduction

Despite many years of studies on scintillating materials many questions are still open. While luminescence processes and high energy radiation interactions with matter are well understood, the fundamental processes of energy transport and high density quenching are still puzzling [1–6]. It is well known that a scintillation pulse shape changes with change of type of excitation ( $\gamma$ -rays, neutrons,  $\alpha$  particles, high energy ions) [7–13]. This phenomenon is commonly used for particle discrimination in variety of applications [14–17]. However, the origin and the exact mechanism are still not known. In last years, a dependence of a

17 scintillation pulse shape on  $\gamma$  photons energy was reported for various materials  
18 [18–21]. Recent theoretical developments [2, 3, 5, 6] provided an explanation of  
19 these observations by modeling the charge separation inside the ionization track  
20 created during a gamma energy excitation.

21 Despite successful results of the theoretical modeling, many aspects still  
22 require an experimental study and verification. This raises a need for new data  
23 and a new experimental approach. The aim of this study is to provide a new  
24 method of characterizing scintillators in two domains simultaneously: in terms  
25 of the excitation energy, and time evolution of scintillation.

26 We will demonstrate that by digitization of individual scintillation pulses and  
27 digital signal processing it is possible to study the scintillation mechanism in  
28 terms of pulse shape and light yield at the same time. For each scintillation pulse  
29 it is possible to calculate the integral light output and corresponding deposited  
30 amount of energy. The acquired pulse height spectrum can be later subdivided  
31 into energy bins. An average scintillation pulse shape can be calculated for  
32 each energy bin by taking an average of all acquired events within that bin.  
33 However, to obtain undistorted pulse shapes additional signal processing and  
34 event selections are required before taking the average.

35 With this method we verified previous experimental results on CsI(Tl) pulse  
36 shape dependence on gamma energy, and we compared those results with the-  
37 oretical models [6]. We have found that the pulse shape change predicted by  
38 the model is in good agreement with the measured data, however we observed  
39 some differences. The proposed method was used to characterize a scintillation  
40 decay time of CsI(Tl) excited with pulsed X-rays and gamma rays. It was found  
41 that X-ray excited pulses have a significantly different pulse shape. We will  
42 conclude that the proposed method provides a new way of characterization of  
43 scintillators.

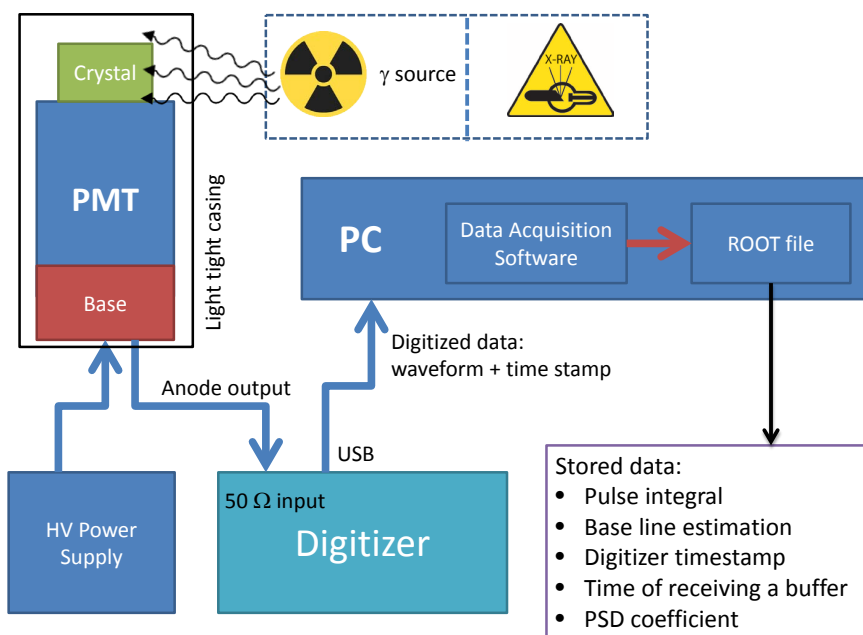


Figure 1: Schematic of the Time Resolved Gamma Spectroscopy setup. The gamma source or a pulsed X-ray tube excite the scintillation crystal. The resulting scintillation pulses are detected with a photomultiplier tube and digitized on event-by-event principle.

## 44 **2. Materials and methods**

### 45 *2.1. The setup*

46 The measuring setup is shown diagrammatically in Fig. 1. Scintillation  
47 pulses from a one inch CsI(Tl) sample are converted to electrical pulses by a  
48 Hamamatsu H5510 Photomultiplier Tube (PMT). The scintillation crystal is  
49 optically coupled with silicon oil to the PMT's entrance window. The PMT's  
50 anode signal is connected directly to the 10-bit 4 Giga Samples Per Second  
51 (GSPS) DT5761 digitizer from CAEN. The digitizer has an input range of 1 Vpp,  
52 input impedance  $Z_{in} = 50 \Omega$ , and a memory buffer depth of  $7.2 \cdot 10^6$  samples.  
53 No preamplifier nor other ways of analog signal shaping have been used. All  
54 data acquisition and on-line processing is done with a personal computer and  
55 homemade software *veroDigitizer*.

56 A  $^{137}\text{Cs}$  source has been used for excitation. The barium X-rays ( 32 keV)  
57 were absorbed by a lead absorber placed between the  $^{137}\text{Cs}$  source and the  
58 detector. In this way we avoided photoelectric absorption of low energy X-  
59 rays, and either photoelectrons or Compton electrons from 662 keV gamma  
60 interaction were detected. As an alternative to  $\gamma$  rays, we used a light excited  
61 X-ray tube N5084 from Hamamatsu for generation of ultra short X-ray pulses  
62 ( $<100$  ps). The X-ray tube has a tungsten target and is powered with a 40 kV  
63 power supply. Each X-ray pulse contains multiple X-ray photons, which enables  
64 low energy excitation ( $\sim 10$  keV) but with a high light output.

### 65 *2.2. Data acquisition*

66 When the anode signal exceeds the digitizer's trigger voltage  $V_{tr}$  an event is  
67 triggered and stored in a local buffer. Each event contains a waveform consisting  
68 of 56k voltage samples ( $14 \mu\text{s}$  time range). When the internal buffer is full, all  
69 digitized events are transferred to the PC for data processing. In order to record  
70 low energy events, the digitizer's trigger voltage  $V_{tr}$  was set as close as possible  
71 to the signal's base line. However, the low  $V_{tr}$  results in pick-up of noise spikes  
72 like in the exemplary pulse shown in Fig. 2. Fig. 3 shows the steps of the

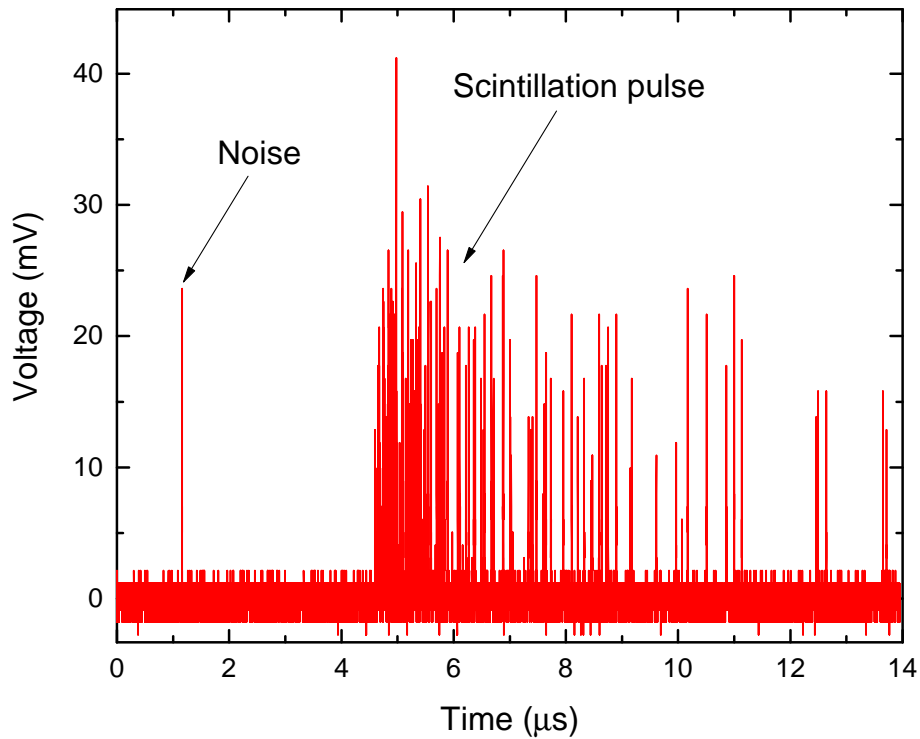


Figure 2: Event triggered by a noise spike at around  $1 \mu\text{s}$  with a coincident scintillation pulse starting at around  $5 \mu\text{s}$ .

73 data processing which are required before the triggered events can be used for  
 74 calculating average pulse shapes. Only events fulfilling multiple criteria are  
 75 selected in order to remove unwanted noise events, suppress pile-up, and assure  
 76 good quality of each triggered pulse. The following sections will discuss in detail  
 77 each step of the data processing.

### 78 *2.3. Filtering and decimation*

79 The digitizer reduces a continuous-time signal from the PMT to a discrete-  
 80 time digital signal (sampling). High sampling frequency of the used digitizer  
 81  $f_s = 4 \text{ GHz}$  provides precise timing information, but in case of CsI(Tl) with  
 82 slow decay time it results in high uncertainty of each value at a point in time  
 83 of the measured signal (low signal to noise ratio), see Fig. 2 and raw signal

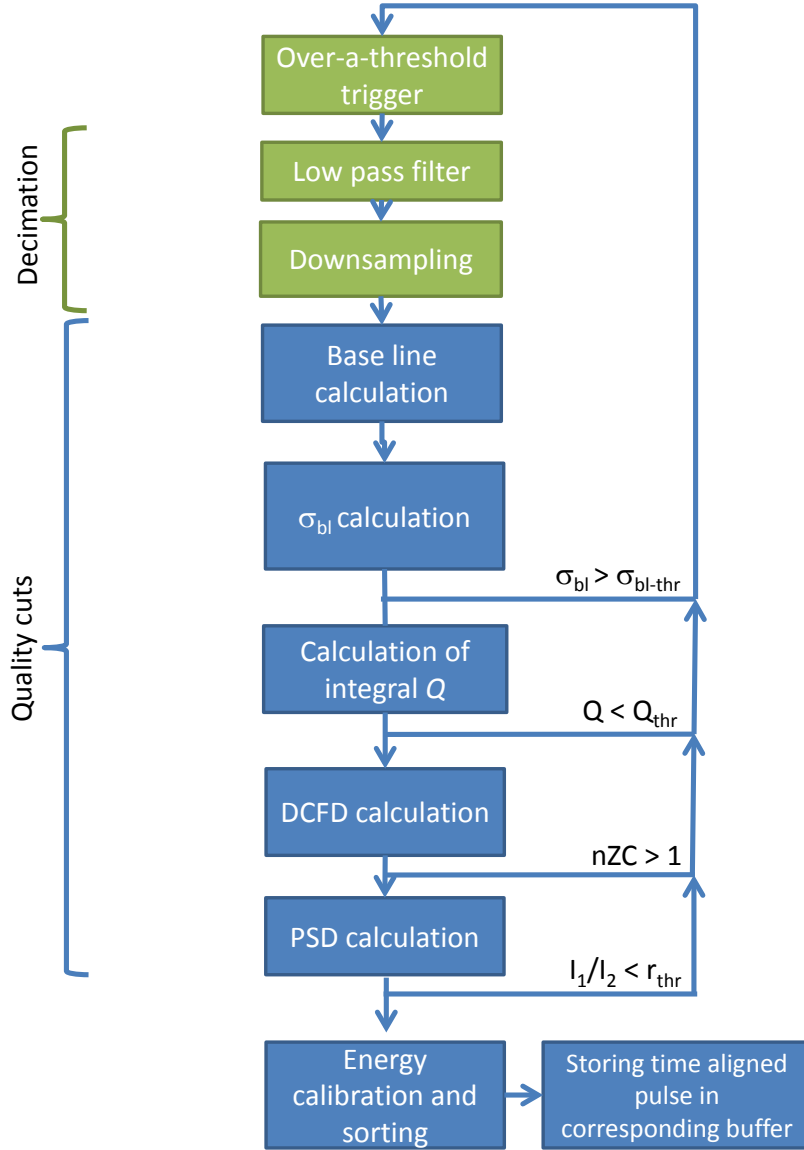


Figure 3: Diagram of data processing workflow.  $\sigma_{bl}$  is the standard deviation of the base line;  $\sigma_{bl-thr}$  is a maximum threshold for standard deviation of the base line;  $Q$  is the pulse integral;  $Q_{thr}$  is a pulse integral minimum threshold;  $nZC$  is the number of zero crossings in the Digital Constant Fraction Discriminator (DCFD) signal;  $I_1/I_2$  is the pulse shape factor defined as the ratio of the short and long integration gates.

84 in Fig. 5. To increase the signal to noise ratio and decrease the uncertainty  
 85 of a measured voltage each waveform was down-sampled (decimated) by first  
 86 applying a low pass digital filter and then reducing the number of samples by a  
 87 factor of  $M = 256$ .

88 To avoid aliasing it is needed to do a low pass filtering before downsampling  
 89 [22]. The cutoff frequency of the filter has to be equal or lower than the Nyquist  
 90 frequency of the down-sampled signal, which is  $f_{co} = \frac{f_s/2}{M} = \frac{4000/2}{256} \approx 7.8$  MHz.  
 91 Fig. 4 shows time and frequency domain responses of multiple standard digital  
 92 filters designed for -3dB cutoff frequency at 7.8 MHz. Because in our measure-  
 93 ments we want to preserve an undistorted time response of the signal, the filter  
 94 choice is limited just to two filters: a moving average filter (length  $N = 227$ ) or a  
 95 Bessel filter. The moving average filter has the worst frequency response among  
 96 considered filters. It has side lobes in the stop band, but provides the fastest  
 97 rise time in response to the step input, and it is free of overshoots in the time  
 98 domain. In addition, a recursive implementation of the moving average filter  
 99 provides the shortest computation time compared to that of the other filters  
 100 [22].

101 Each sample of the downsampled waveform  $d[i]$  is calculated by taking the  
 102 average value of length  $M = 256$  from the filtered waveform  $f[i]$  according to  
 103 the formula:  $d[i] = \frac{1}{M} \sum_{k=M \cdot i}^{M \cdot (i+1)} f[k]$ .

#### 104 2.4. Quality cuts

105 Selections were applied to data to remove noise events, assure proper trigger-  
 106 ing time within each waveform, and to select non distorted single scintillation  
 107 pulses. Fig. 3 shows the steps of the data processing. After an event decimation  
 108 a baseline  $BL$  and its' standard deviation  $\sigma_{bl}$  are calculated. If  $\sigma_{bl}$  exceeds the  
 109 base line standard deviation threshold  $\sigma_{bl-thr}$  the event is discarded and no  
 110 longer processed. In this way we assure a good quality of the calculated base  
 111 line. Usually  $\sigma_{bl-thr}$  is exceeded when random noise is present within the base  
 112 line window or a scintillation pulse was triggered too late and the leading edge  
 113 is before the expected triggering time.



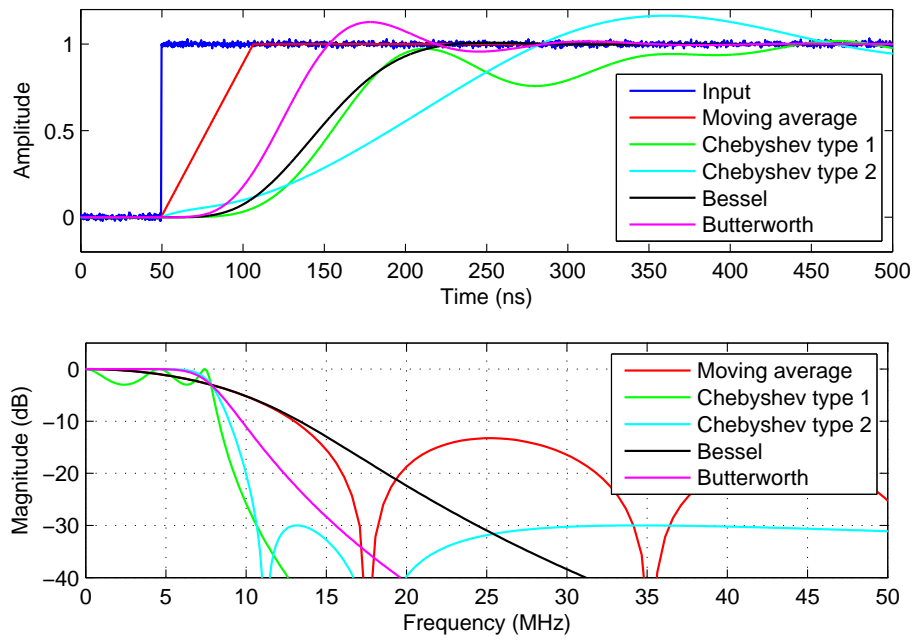


Figure 4: Comparison of five digital low pass filters in time (upper panel) and frequency domains (lower panel).

114 In the next step the integral  $Q$  of a decimated pulse is calculated using the  
115 previously obtained base line:  $Q = \sum_0^L (w[i] - BL)$ . If the calculated  $Q$  is lower  
116 than the minimum integral threshold  $Q_{thr}$ , the event is discarded and no longer  
117 processed. This requirement suppresses all events which exceed the digitizer's  
118 trigger threshold, but consist mostly of noise spikes, single photoelectron events,  
119 afterglow pulses, or other non-scintillation pulses. This requirement is crucial  
120 especially for low energy deposition events when noise is of the same order of  
121 magnitude as the scintillation pulses. If not suppressed properly it can lead to  
122 creation of an artificial fast component in a decay spectrum or other distortions  
123 of a pulse shape.

124 Fig. 2 shows an example of a "wrong" event: a scintillation pulse appears  
125 after the expected trigger point. A noise peak exceeded the trigger threshold  
126 and the event was digitized and stored. The scintillation pulse which coincided  
127 with the noise pulse caused that the event passed minimum energy requirement.  
128 However, the leading edge of the scintillation pulse is not properly located in  
129 the time window.

130 To properly measure a pulse shape it is important to suppress pile-up of  
131 scintillation events within the acquisition window. In Fig. 5 the black line  
132 shows a raw signal from the digitizer; the red line shows the signal after low  
133 pass filtering and downsampling; the blue line shows the output of a digital  
134 constant fraction discriminator (DCFD). There are two points in the figure when  
135 the DCFD signal is crossing zero, which indicates that we are dealing with two  
136 scintillation pulses. If more than one zero crossing  $n_{ZC} > 1$  was observed within  
137 the acquisition window the event was rejected from further processing. If only  
138 one zero crossing was observed the event was kept for further processing, and  
139 the zero crossing time was used later for aligning events in time.

### 140 3. Results

141 Fig. 6 shows a pulse height spectrum measured with CsI(Tl) excited with  
142 662 keV  $\gamma$ -photons. The barium x-ray peak was successfully suppressed by the

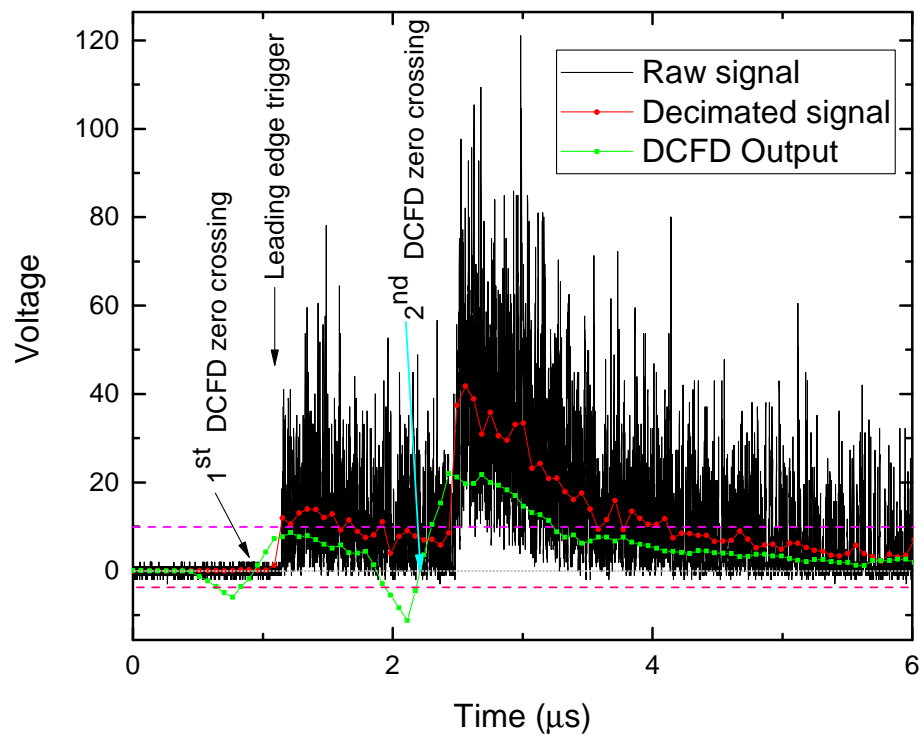


Figure 5: Exemplary pile-up event.

143 lead absorber, and only Compton scattered events are present besides the 662  
144 keV photopeak. The shown energy range was divided into 10 energy bins and  
145 an average pulse shape for each range has been calculated separately.

146 Fig. 7 shows pulse shapes of CsI(Tl) scintillation measured in multiple en-  
147 ergy subranges. The only curve that deviates significantly is for 25-97 keV  
148 energies. Another measurement was performed with the requirement that the  
149 energy deposit is lower than 184 keV to investigate better the low energy range.  
150 Fig. 8 shows the decay curves at low energy deposition. The largest difference  
151 was observed for 25-41 keV events, a very small deviation was observed in the  
152 41-89 keV range, and small but still rousignificant pulse change was observed  
153 from 89 keV to 184 keV.

154 To quantify the pulse shape change shown in Fig. 8, the decay curves were  
155 fitted with a double exponential function  $f(t) = A_1 \exp(-\frac{t}{\tau_1}) + A_2 \exp(-\frac{t}{\tau_2})$ ,  
156 where  $A_1$  and  $A_2$  are the amplitudes of the fast and the slow component, and  
157  $\tau_1$  and  $\tau_2$  are decay constants. The results of these fits are shown in Fig. 9 and  
158 Fig. 10, where intensities  $I_1$  and  $I_2$  were calculated as follows:  $I_i = \frac{A_i * \tau_i}{A_1 * \tau_1 + A_2 * \tau_2}$ .  
159 Both decay constants are decreasing with decrease of energy, but there is a 'dip'  
160 present near 60 keV. The slow component decreases from around 5.8  $\mu$ s to 4.7  
161  $\mu$ s in the studied energy range, while the fast component changes from around  
162 900 ns to 850 ns.

163 The intensity of the slow component  $I_2$  increases with increase of energy, see  
164 Fig. 10. The intensity change deviates from being smooth at energies around  
165 50 keV, similarly to the decay components.

166 Fig. 11 shows a pulse height spectrum measured with a  $^{137}\text{Cs}$  source together  
167 with X-ray pulses from a pulsed X-ray tube. The tube pulses are observed at  
168 deposited energy of around 1.3 MeV with FWHM of 37%. Assuming that the  
169 average energy of a single X-ray photon from the tungstate anode is around  $\sim 10$   
170 keV, we may estimate that a single X-ray pulse leads to  $\sim 130$  detected x-ray  
171 photons.

172 Fig. 12 compares a scintillation pulse shape of CsI(Tl) excited with high  
173 energy gamma photons (575-758 keV), low energy Compton electrons (25-96

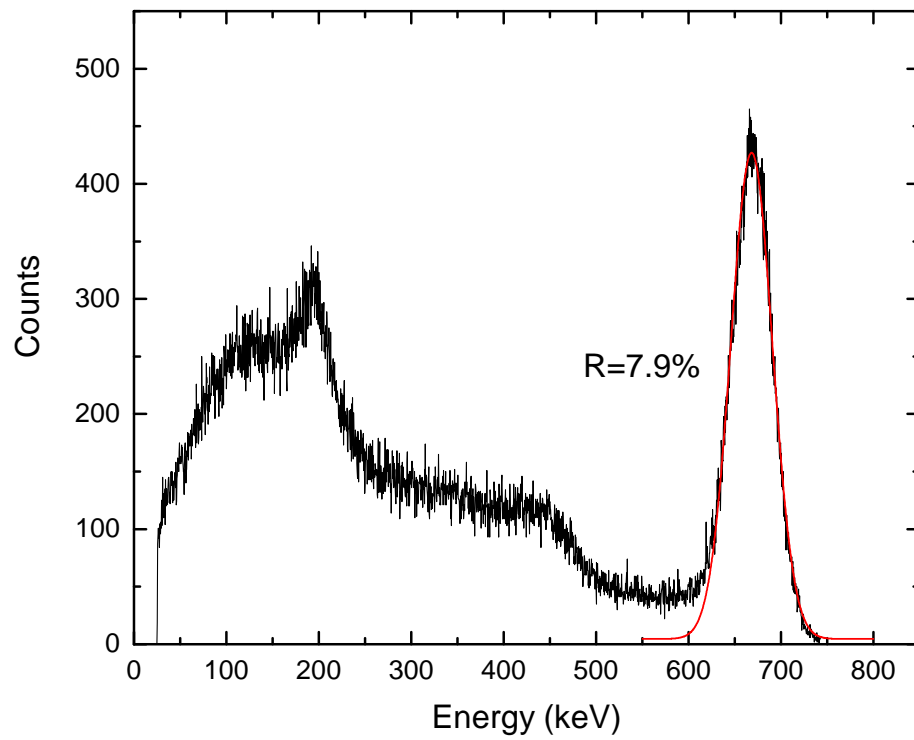


Figure 6: Pulse height spectrum of  $^{137}\text{Cs}$  gamma source measured with CsI:Tl.

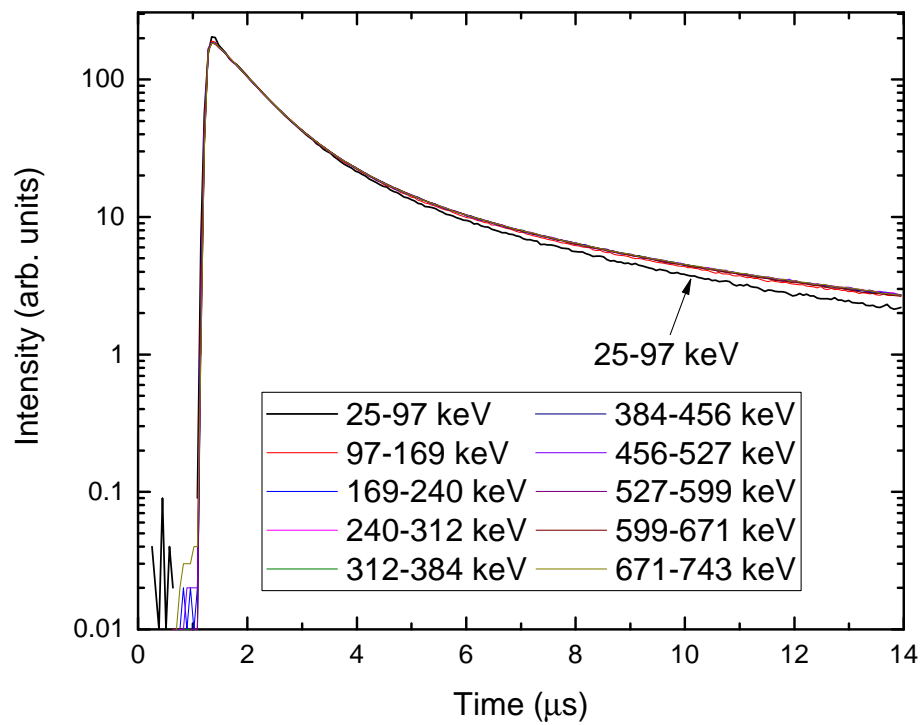


Figure 7: Energy-sorted pulse shapes of CsI(Tl) under Cs-137 excitation. Only the lowest energy range 25-97 keV displays a significantly different pulse shape.

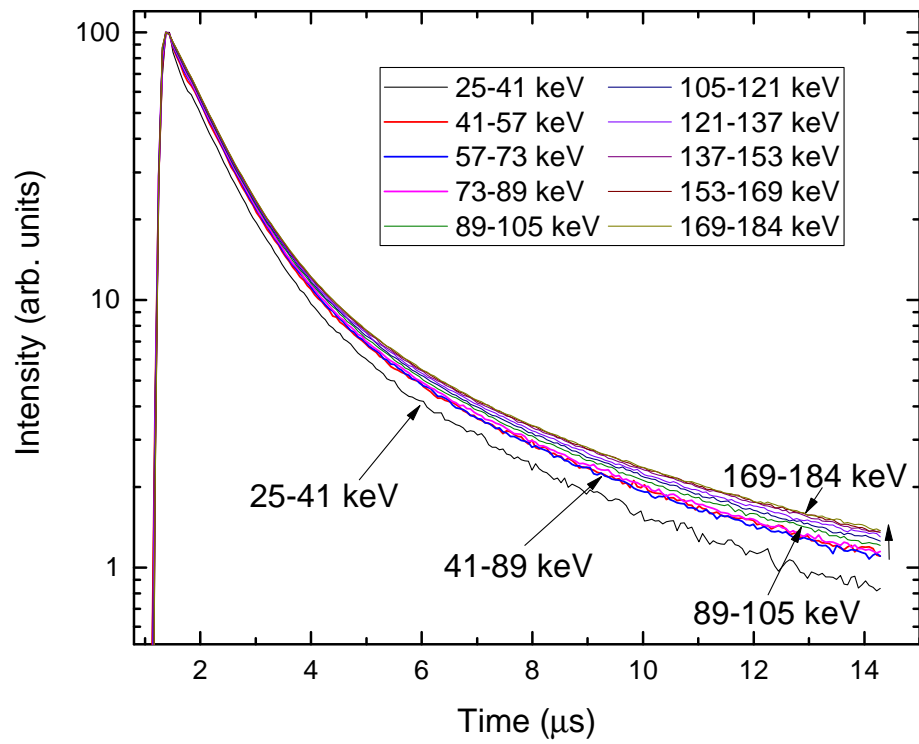


Figure 8: Energy-sorted pulse shapes of CsI(Tl) under Cs-137 excitation, events with energies lower than 228 keV.

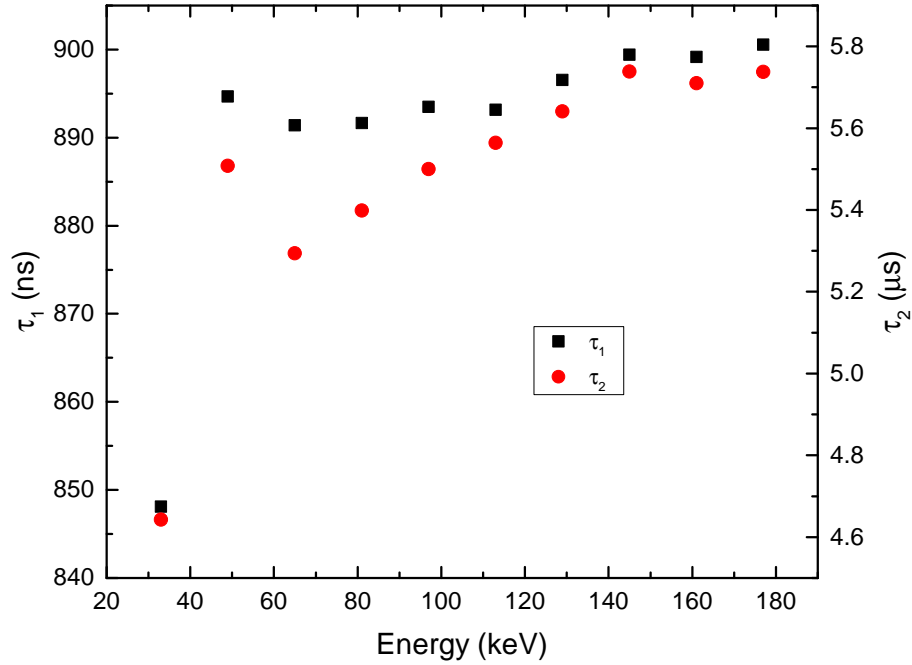


Figure 9: Decay constants of fast  $\tau_1$  and  $\tau_2$  slow luminescence decay components.

174 keV), and picosecond X-ray pulses (10 keV). Events excited by the pulsed x-  
 175 ray tube exhibit the lowest intensity of the long decay component, while high  
 176 energy  $\gamma$  photons have the highest intensity of the slow component. The pulses  
 177 from Fig. 12 were fitted with a double exponential function and the results  
 178 are shown in Table 1. The fast component under X-ray excitation is 6% faster  
 179 compared to the 662 keV energy range. The slow decay constant decreases  
 180 11% in the same energy range. The intensity of the slow component increases  
 181 4.3% when the source of excitation is changed from 662 keV to X-rays. The  
 182 pulse change measured with low energy deposition (25-97 keV) compared to the  
 183 575-758 keV range is significantly smaller and it is less than 1% change of the  
 184 fast decay component and less than 4% of the slow component. The change of  
 185 intensity is around 1%.

186 The pulse shape factor was defined as a ratio of two integrals: the leading  
 187 edge, and the tail part of the pulse. Length of both integrals was optimized to



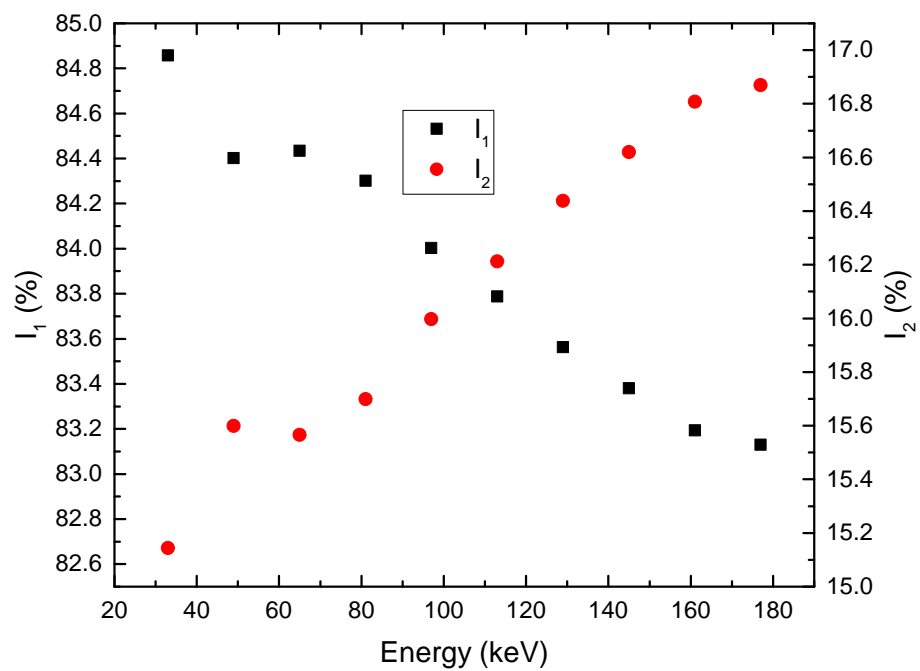


Figure 10: Intensities of fast  $I_1$  and slow  $I_2$  luminescence decay components.

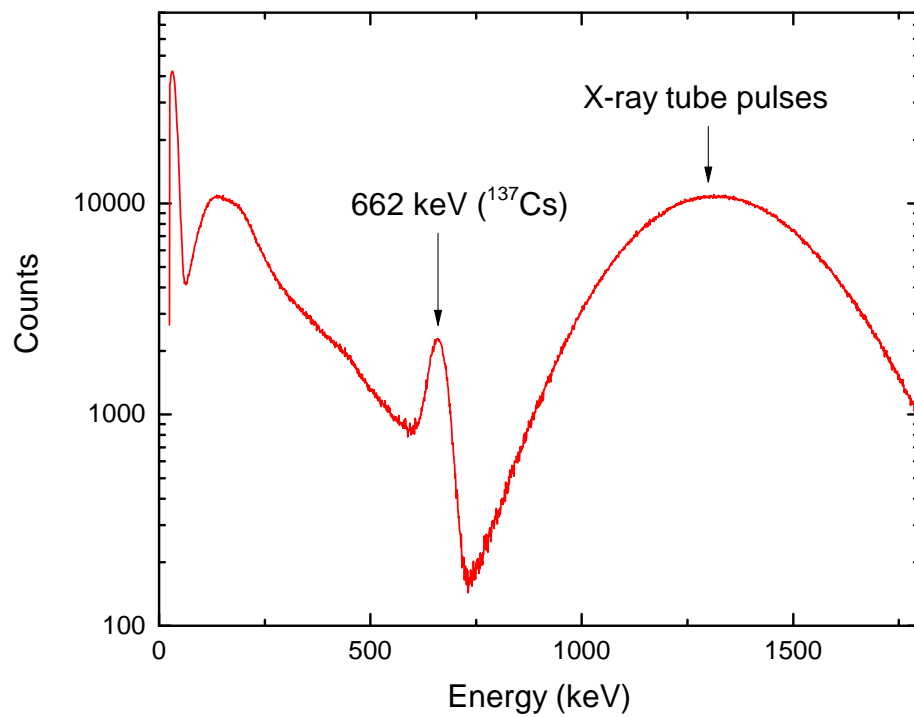


Figure 11: Pulse height spectrum measured with CsI(Tl) excited with a Cs-137 gamma source and pulsed X-ray tube.

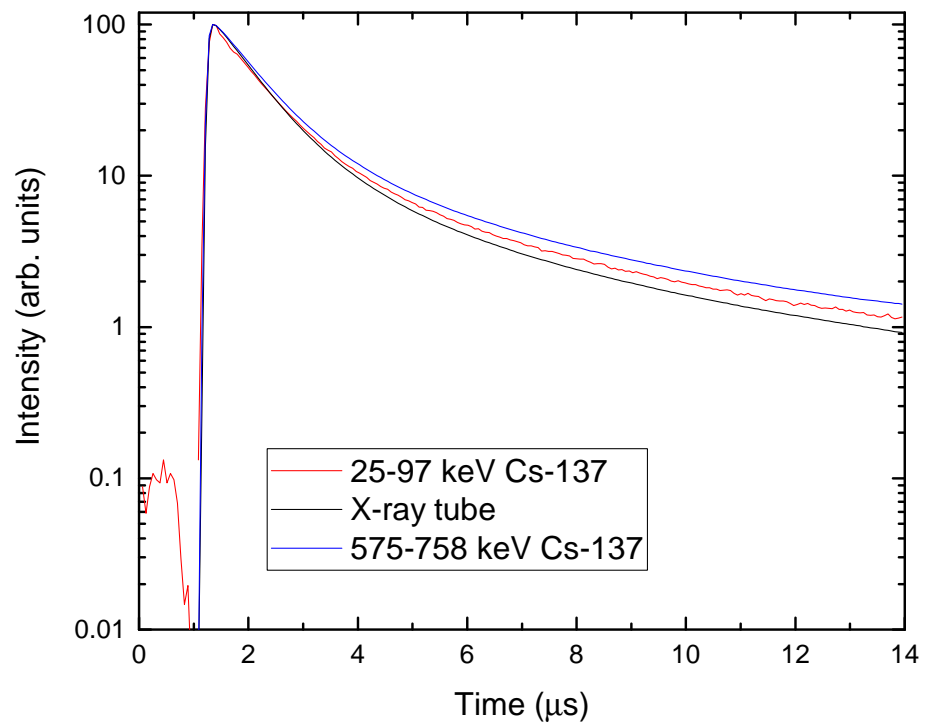


Figure 12: Comparison of CsI(Tl) scintillation pulse shape excited with Cs-137 gamma source and picosecond X-ray tube pulses.

Table 1: Decay constants and their intensities of CsI(Tl) luminescence excited with a picosecond X-ray tube, low and high energy excitation.

Excitation	$\tau_1$ (ns)	$\tau_2$ ( $\mu$ s)	$I_1$ (%)	$I_2$ (%)
X-rays	800	4.7	87.1	12.9
25-97 keV	845	5.1	83.9	16.1
575-758 keV	850	5.3	82.8	17.2

188 get the pulse shape factor value close to one. Fig. 13 shows pulse shape factor  
 189 versus energy of pulses. X-ray pulses (1000-2200 channels) have higher pulse  
 190 shape factor than  $\gamma$  rays from Cs-137 source (662 keV at 800 channel).

#### 191 4. Discussion

192 Lu et al. [6] provided a detailed theoretical analysis of the pulse shape  
 193 dependence on gamma energy in CsI(Tl). Three possible reactions leading to  
 194 luminescence were considered. Reaction 1 is the direct  $Tl^+$  excitation by sequen-  
 195 tial capture of free holes and electrons:  $Tl^+ + e^- + h^+ \rightarrow (Tl^+)^* \rightarrow Tl^+ + h\nu$ .  
 196 Reaction 2 is the recombination of self-trapped holes with electrons trapped on  
 197  $Tl^0$ :  $Tl^0 + STH \rightarrow (Tl^+)^*$ . Reaction 3 is the thermally activated release of elec-  
 198 trons trapped as  $Tl^0$  that subsequently recombine with holes trapped as  $Tl^{2+}$ :  
 199  $Tl^0 + Tl^{2+} \rightarrow (Tl^+)^*$ . According to Lu et al., the fast  $\sim 700$  ns decay component  
 200 can be mostly attributed to the 576 ns radiative decay of  $(Tl^+)^*$  from Reaction  
 201 2 and to transport limited Reaction 3, while the 3- and 17 $\mu$ s components are  
 202 the rate- and transport limited phases of Reaction 3. The energy dependence  
 203 of the pulse shape can be explained by the change of efficiency of the Reaction  
 204 3 which is dependent on the electric field created between space-separated  $Tl^0$   
 205 and  $Tl^{2+}$  reservoirs.

206 Fig. 14 shows a comparison of the theoretical modeling results by Lu [6] and  
 207 experimental data presented in this work. The model provides a good qualita-  
 208 tive description of the data; the same trend and magnitude of the experimental  
 209 pulse shape change is reproduced by the calculations. However, there are some

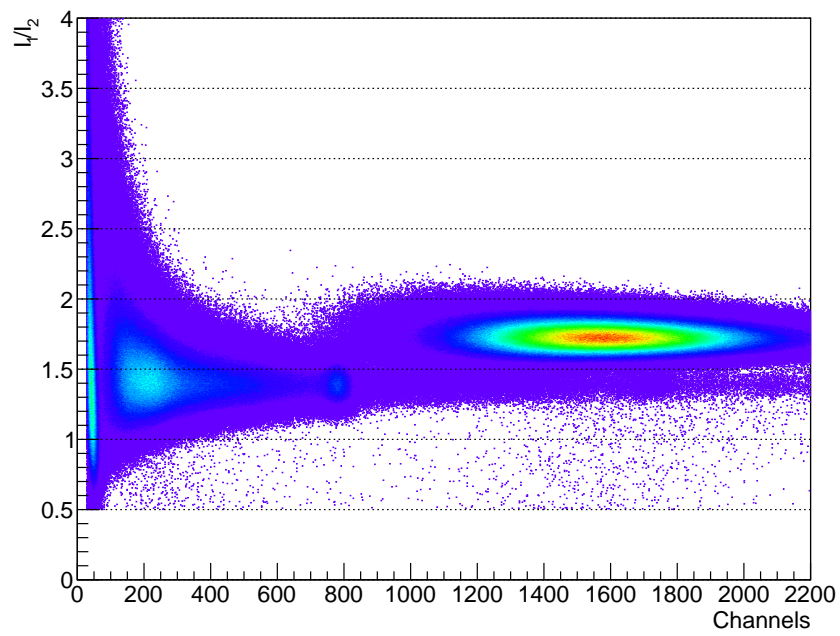


Figure 13: Pulse shape factor vs pulse integral. Scintillation pulses excited with X-ray tube exhibit a distinctively different shape.

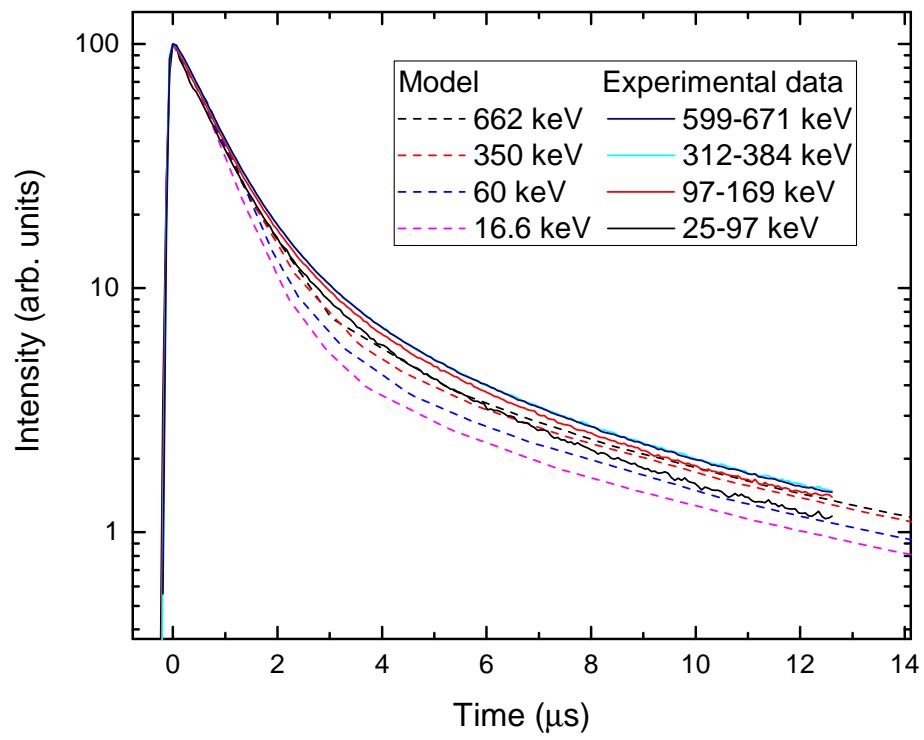


Figure 14: Comparison of the Lu model predictions [6] with the measured data.

210 discrepancies. The model does not predict correctly a change of the slow com-  
211 ponent ( $\sim 5 \mu\text{s}$ ) decay constant, and the change of the fast component ( $\sim 800$   
212 ns) is predicted to be bigger than observed in experiment. Some difficulty for a  
213 fair comparison is caused by the fact that the experimental data are measured  
214 with limited energy resolution ranges, while theoretical predictions are provided  
215 for monoenergetic gamma photons.

## 216 5. Conclusions

217 In this article we have presented a new method of characterizing scintillators.  
218 We found a weak pulse shape dependence on gamma energy for CsI(Tl), and  
219 different scintillation decay time for gamma rays and X-ray pulsed excitations.  
220 The experimental results are in good agreement with theoretical predictions by  
221 Lu et al. [6], but minor differences are observed and require more research.

## 222 6. Acknowledgments

223 This work was supported by the Dutch Technology Foundation STW, which  
224 is part of the Netherlands Organization for Scientific Research (NWO), which  
225 is partly funded by the Ministry of Economic Affairs. This work was partly  
226 funded by Saint Gobain Crystals, France.

227 [1] P. Dorenbos, J. de Haas, and C. van Eijk, “Non-proportionality in the  
228 scintillation response and the energy resolution obtainable with scintillation  
229 crystals,” *IEEE Transactions on Nuclear Science*, vol. 42, pp. 2190–2202,  
230 Dec 1995.

231 [2] R. T. Williams, J. Q. Grim, Q. Li, K. B. Ucer, G. A. Bizarri, S. Kerisit,  
232 F. Gao, P. Bhattacharya, E. Tupitsyn, E. Rowe, V. M. Buliga, and  
233 A. Burger, “Experimental and computational results on exciton/free-  
234 carrier ratio, hot/thermalized carrier diffusion, and linear/nonlinear rate  
235 constants affecting scintillator proportionality,” vol. 8852, pp. 88520J–  
236 88520J–22, 2013.

- 237 [3] J. Q. Grim, K. B. Ucer, A. Burger, P. Bhattacharya, E. Tupitsyn, E. Rowe,  
238 V. M. Buliga, L. Trefilova, A. Gektin, G. A. Bizarri, W. W. Moses, and  
239 R. T. Williams, “Nonlinear quenching of densely excited states in wide-gap  
240 solids,” *Phys. Rev. B*, vol. 87, p. 125117, Mar 2013.
- 241 [4] G. Bizarri, N. J. Cherepy, W. S. Choong, G. Hull, W. W. Moses,  
242 S. A. Payne, J. Singh, J. D. Valentine, A. N. Vasilev, and R. T.  
243 Williams, “Progress in studying scintillator proportionality: Phenomeno-  
244 logical model,” *IEEE Transactions on Nuclear Science*, vol. 56, pp. 2313–  
245 2320, Aug 2009.
- 246 [5] X. Lu, Q. Li, G. A. Bizarri, K. Yang, M. R. Mayhugh, P. R. Menge, and  
247 R. T. Williams, “Coupled rate and transport equations modeling propor-  
248 tionality of light yield in high-energy electron tracks: CsI at 295 K and 100  
249 K; CsI:Tl at 295 K,” *Phys. Rev. B*, vol. 92, p. 115207, Sep 2015.
- 250 [6] X. Lu, S. Gridin, R. T. Williams, M. R. Mayhugh, A. Gektin, A. Syntfeld-  
251 Kazuch, L. Swiderski, and M. Moszynski, “Energy-dependent scintillation  
252 pulse shape and proportionality of decay components for csi:tl: Modeling  
253 with transport and rate equations,” *Phys. Rev. Applied*, vol. 7, p. 014007,  
254 Jan 2017.
- 255 [7] L. Dinca, P. Dorenbos, J. de Haas, V. Bom, and C. V. Eijk, “Alphagamma  
256 pulse shape discrimination in CsI:Tl, CsI:Na and BaF<sub>2</sub> scintillators,” *Nu-  
257 clear Instruments and Methods in Physics Research Section A: Acceler-  
258 ators, Spectrometers, Detectors and Associated Equipment*, vol. 486, no. 12,  
259 pp. 141 – 145, 2002. Proceedings of the 6th International Conference on  
260 Inorganic Scintillators and their Use in Scientific and Industrial Applica-  
261 tions.
- 262 [8] M. Kobayashi, Y. Tamagawa, S. Tomita, A. Yamamoto, I. Ogawa,  
263 and Y. Usuki, “Significantly different pulse shapes for  $\gamma$ - and  $\alpha$ -rays  
264 in Gd<sub>3</sub>Al<sub>2</sub>Ga<sub>3</sub>O<sub>12</sub>:Ce<sup>3+</sup> scintillating crystals,” *Nuclear Instruments and*



- 265 *Methods in Physics Research Section A: Accelerators, Spectrometers, De-*  
266 *tectors and Associated Equipment*, vol. 694, pp. 91 – 94, 2012.
- 267 [9] L. Bardelli, M. Bini, P. Bizzeti, F. Danevich, T. Fazzini, N. Krutyak,  
268 V. Kobychyev, P. Maurenzig, V. Mokina, S. Nagorny, M. Pashkovskii,  
269 D. Poda, V. Tretyak, and S. Yurchenko, “Pulse-shape discrimination with  
270  $\text{PbWO}_4$  crystal scintillators,” *Nuclear Instruments and Methods in Physics*  
271 *Research Section A: Accelerators, Spectrometers, Detectors and Associated*  
272 *Equipment*, vol. 584, no. 1, pp. 129 – 134, 2008.
- 273 [10] K. Yang, P. R. Menge, and V. Ouspenski, “Enhanced  $\alpha$  -  $\gamma$  discrimination  
274 in co-doped  $\text{LaBr}_3:\text{Ce}$ ,” *IEEE Transactions on Nuclear Science*, vol. 63,  
275 pp. 416–421, Feb 2016.
- 276 [11] S. Rawat, M. Tyagi, P. Netrakanti, V. Kashyap, A. Singh, D. Desai, A. Mi-  
277 tra, G. A. Kumar, and S. Gadkari, “Pulse shape discrimination properties of  
278  $\text{Gd}_3\text{Ga}_3\text{Al}_2\text{O}_{12}:\text{Ce,B}$  single crystal in comparison with  $\text{CsI:Tl}$ ,” *Nuclear In-*  
279 *struments and Methods in Physics Research Section A: Accelerators, Spec-*  
280 *trometers, Detectors and Associated Equipment*, pp. –, 2016.
- 281 [12] K. Mesick, D. Coupland, and L. Stonehill, “Pulse-shape discrimination and  
282 energy quenching of alpha particles in  $\text{Cs}_2\text{LiLaBr}_6:\text{Ce}^{3+}$ ,” *Nuclear Instru-*  
283 *ments and Methods in Physics Research Section A: Accelerators, Spectrom-*  
284 *eters, Detectors and Associated Equipment*, vol. 841, pp. 139 – 143, 2017.
- 285 [13] N. Zaitseva, B. L. Rupert, I. Paweczak, A. Glenn, H. P. Martinez, L. Car-  
286 man, M. Faust, N. Cherepy, and S. Payne, “Plastic scintillators with ef-  
287 ficient neutron/gamma pulse shape discrimination,” *Nuclear Instruments*  
288 *and Methods in Physics Research Section A: Accelerators, Spectrometers,*  
289 *Detectors and Associated Equipment*, vol. 668, no. Supplement C, pp. 88 –  
290 93, 2012.
- 291 [14] P. Belli, R. Bernabei, R. Cerulli, C. Dai, F. Danevich, A. Incicchitti,  
292 V. Kobychyev, O. Ponkratenko, D. Prospero, V. Tretyak, and Y. Zdesenko,

- 293 “Performances of a  $\text{CeF}_3$  crystal scintillator and its application to the search  
294 for rare processes,” *Nuclear Instruments and Methods in Physics Research*  
295 *Section A: Accelerators, Spectrometers, Detectors and Associated Equip-*  
296 *ment*, vol. 498, no. 13, pp. 352 – 361, 2003.
- [15] R. Ogawara and M. Ishikawa, “Feasibility study on signal separation for  
297 spontaneous alpha decay in  $\text{LaBr}_3\text{:Ce}$  scintillator by signal peak-to-charge  
298 discrimination,” *Review of Scientific Instruments*, vol. 86, no. 8, 2015.  
299
- [16] C. M. Whitney, L. Soundara-Pandian, E. B. Johnson, S. Vogel, B. Vinci,  
300 M. Squillante, J. Glodo, and J. F. Christian, “Gammaneutron imaging  
301 system utilizing pulse shape discrimination with clyc,” *Nuclear Instruments*  
302 *and Methods in Physics Research Section A: Accelerators, Spectrometers,*  
303 *Detectors and Associated Equipment*, vol. 784, no. Supplement C, pp. 346 –  
304 351, 2015. Symposium on Radiation Measurements and Applications 2014  
305 (SORMA XV).  
306
- [17] R. Cerulli, P. Belli, R. Bernabei, F. Cappella, F. Nozzoli, F. Montecchia,  
307 A. d’Angelo, A. Incicchitti, D. Prosperi, and C. Dai, “Performances of a  
308  $\text{BaF}_2$  detector and its application to the search for decay modes in  $^{130}\text{Ba}$ ,”  
309 *Nuclear Instruments and Methods in Physics Research Section A: Acceler-*  
310 *ators, Spectrometers, Detectors and Associated Equipment*, vol. 525, no. 3,  
311 pp. 535 – 543, 2004.  
312
- [18] A. Syntfeld-Kazuch, M. Moszyński, L. Świdorski, W. Klamra, and A. Nas-  
313 salski, “Light pulse shape dependence on  $\gamma$ -ray energy in  $\text{CsI(Tl)}$ ,” *IEEE*  
314 *Transactions on Nuclear Science*, vol. 55, pp. 1246–1250, June 2008.  
315
- [19] W.-S. Choong, G. Bizarri, N. Cherepy, G. Hull, W. Moses, and S. Payne,  
316 “Measuring the dependence of the decay curve on the electron energy de-  
317 posit in  $\text{NaI(Tl)}$ ,” *Nuclear Instruments and Methods in Physics Research*  
318 *Section A: Accelerators, Spectrometers, Detectors and Associated Equip-*  
319 *ment*, vol. 646, no. 1, pp. 95 – 99, 2011.  
320

- 321 [20] X. Wen and A. Enqvist, “Measuring the scintillation decay time for dif-  
322 ferent energy deposited by  $\gamma$ -rays and neutrons in a  $\text{Cs}_2\text{LiYCl}_6:\text{Ce}^{3+}$  de-  
323 tector,” *Nuclear Instruments and Methods in Physics Research Section A: Accelerators, Spectrometers, Detectors and Associated Equipment*, vol. 853,  
324 no. Supplement C, pp. 9 – 15, 2017.
- 326 [21] L. Świdorski, n. Marek Moszy A. Syntfeld-Kazuch, M. Szawłowski, and  
327 T. Szcześniak, “Measuring the scintillation decay time for different energy  
328 depositions in NaI:Tl, LSO:Ce and  $\text{CeBr}_3$  scintillators,” *Nuclear Instru-*  
329 *ments and Methods in Physics Research Section A: Accelerators, Spectrom-*  
330 *eters, Detectors and Associated Equipment*, vol. 749, no. Supplement C,  
331 pp. 68 – 73, 2014.
- 332 [22] S. W. Smith, *The Scientist and Engineer’s Guide to Digital Signal Process-*  
333 *ing*. San Diego, CA, USA: California Technical Publishing, 1997.